A Deep Radio Survey of Abell 2125 I.

Radio, Optical and Near-IR Observations

Frazer N. Owen,[1,2], W. C. Keel,[3,2], M. J. Ledlow[4,2,5] G. E. Morrison,[6,2], & R. A. Windhorst[7,2]

ABSTRACT

We present a description of deep radio, optical, and near IR observations taken with the VLA, the KPNO 2m and the KPNO 4m of the region containing the rich cluster of galaxies Abell 2125. The reduction of each dataset is described. A catalog of radio sources apparently not associated with members of Abell 2125 and the associated R-band magnitudes is presented.

Subject headings: cosmology: observations — galaxies: evolution — galaxies: starburst — infrared: galaxies galaxies: clusters: individual (Abell 2125)

1. Introduction

Deep radio observations offer one of the important windows on the evolution of star formation and black-hole-related activity as a function of cosmological epoch. Radio, optical/NIR, FIR and X-ray data taken together have the potential eventually to give us a well-constrained picture of our history. Each window, by itself, has serious weaknesses. The

---

[1]National Radio Astronomy Observatory, P. O. Box O, Socorro, NM 87801 USA.; fowen@nrao.edu The National Radio Astronomy Observatory is facility of the National Science Foundation operated under cooperative agreement by Associated Universities Inc.

[2]Visiting astronomer, Kitt Peak National Observatory, National Optical Astronomy Observatories, operated by AURA, Inc., under cooperative agreement with the National Science Foundation.

[3]Dept. of Physics & Astronomy, University of Alabama, Tuscaloosa, AL 35487 USA

[4]Gemini Observatory, Southern Operations Center, AURA, Casilla 603, La Serena, Chile

[5]Deceased 5 June 2004. We shall miss his cheerfulness, unfailing good sense, and scientific industry.

[6]National Optical Astronomy Observatories, 950 N. Cherry Ave., Tucson, AZ 85719 USA

[7]Arizona State University, Dept. of Physics & Astronomy, Tyler Mall PSF-470, Box 871504, Tempe, AZ 85287-1504 USA

optical/NIR window is the best studied and provides the most direct view. However, it suffers from uncertainties due to dust obscuration, a fundamental part of star-formation. FIR observations give us a signal from the dust but leave uncertain the origin of heating of the dust and fail to see into the heart of the AGN or star-forming regions. In X-rays and radio we can see behind the dust but we are measuring secondary emission which is not easy to relate physically to the black hole physics or star-formation-rate (SFR). Thus we need a combination of all this information to deduce the full picture.

Below $L_{20cm} \sim 10^{23}$ W Hz^{-1}, one can show that locally the radio luminosity function is dominated by synchrotron emission related to star-formation driven processes (e.g., Condon 1992). Above this luminosity most sources are twin-jet, black-hole-driven sources. Below the 10^{23} W Hz^{-1} break point, the sources are mostly found in spirals rather than ellipticals and the radio and FIR luminosities correlate very well (e.g., Yun, Reddy, & Condon 2001). Through the radio-FIR correlation, one can estimate the SFR for the radio alone and can use the ratio of radio to submillimeter emission to constrain the redshift (assuming the empirical radio-FIR relation continues to hold at any redshift) (Carilli & Yun 1999). Thus deep radio observations with limiting flux densities $<< 1$ mJy, offer a way to study star formation in the distant universe.

However, there are a lot of assumptions in the previous paragraph. What one really needs is deep data in all four windows to understand the picture. Where we have such information new puzzles arise. For example, SCUBA submillimeter sources are usually associated with faint radio sources. Using the superior radio positions, one can make faint optical identifications and try to measure redshifts. Often when an optical redshift can be obtained, one finds an AGN spectrum (e.g., Ledlow et al. 2002). Even so, the redshift estimated from the Carilli/Yun relation agrees with the measured value. Perhaps this is a coincidence but it might suggest that bright black-hole-driven AGN's are part of the star-formation process in galaxies.

We are interested both in the very distant star-formation/AGN history as well as the same phenomena in intermediate-distance rich clusters($0.2 \lesssim z \lesssim 0.4$). A deep radio survey in the direction on such a cluster can be used for both purposes. This paper reports deep radio observations in the direction of Abell 2125. Future papers will report the combination of these data with observations in other bands to study both problems.

We began studying the Abell 2125 field with medium deep, 20cm, VLA C-array observations (Dwarakanath & Owen 1999; Owen et al. 1999). We compared Abell 2125 (a richness class 4, blue cluster and $z \sim 0.25$) with Abell 2645 (an apparently similar cluster at the same redshift but with much redder galaxies). We found a much higher detection rate of radio galaxies (27 vs 4) in Abell 2125. The detection rate in A2645 is consistent with a normal AGN population in a lower redshift cluster. The A2125 excess population occurs entirely with luminosities below $L_{20cm} \sim 10^{23}$ W Hz^{-1} and thus seems consistent with a star-forming population. However, only a small fraction of the excess population have optical spectra consistent with enough star-formation activity to explain the population entirely that way. Either the star-forming activity is very well hidden in the majority of the low radio luminosity sample or the some other explanation is necessary for the radio activity.

One possible clue is that Abell 2125 does not appear to be a typical very rich cluster when examined in more detail in the optical and X-ray bands. Optically the cluster consists of a central concentration together with a extension to the southwest extending at least 2 Mpc. X-ray observations (Wang, Connolly, & Brunner 1997) show the same pattern and that the total X-ray luminosity is low for such a rich cluster. Much of the excess X-ray population is contained in the southwest extension, not the cluster core. Thus perhaps these unusual properties have something to do with the radio excess.

To study the cluster further, we have made a much deeper radio observations and higher resolution using all four VLA configurations. The deep radio data has also motivated deep optical and NIR imaging, optical spectroscopy (Miller et al 2004), deep millimeter/submillimeter observations (Eales et al 2003), and a deep *Chandra* exposure (Wang, Owen & Ledlow 2004).In some cases, these ancillary observations were not motivated by the cluster but by the possibility of studying the background sample (*e.g.* the submillimeter survey). In this paper we document the techniques used in reducing the radio and optical imaging data for this field. We also report the radio data and R-band optical identifications for these data. A related paper contains the results for the radio sources confirmed to be associated with cluster members.

2. Observations, Reduction and Cataloging

Observations were made with the VLA for 3.5 hours in the 1997 B configuration and for 27.5 hours in the 1998 A configuration. Since the total time is dominated by the A configuration, the final image for analysis had a resolution about 1.5 arcsec. The data were all taken in spectra line mode 4, which provides seven 3.125 MHz channels in each of 2 IFs (centered at 1365 and 1435 MHz) and each of two polarizations. Five second integration times were used in the A and B array. The integration times and channel bandwidths were chosen to minimize tangential and radial smearing of the images away from the field center. It would be better to use narrower channel widths, and shorter integration times to eliminate such effects totally but the mode we picked seems the best compromise given the current VLA correlator and data handling system. Another important consideration for deep VLA work at 20cm with the present system is that the system temperature increases as function of zenith distance due to increased ground pickup. For this reason almost all the observations were scheduled within 3 hours of source transit to minimize this effect.

2.1. Calibration & Editing

All radio reductions use the AIPS package. Since the total bandwidth is relatively large for a spectral line experiment, for each daily observation we first split a bright point source calibrator from the raw database and applied a phase self-calibration. Then we used this otherwise, uncalibrated source to calculate a bandpass correction before we proceeded with the rest of the regular continuum calibration. Regular continuum calibration then continued, using the bandpass calibration to flatten the spectral response, and thus avoid the effects of the raw, sloping spectral response. Calibration was made in the standard way to the Baars flux density scale using 3C286 as the flux calibrator. The weights associated with each integration were also calibrated as a function of observed system temperature and calibrated as part of the standard AIPS processing. The calibrated dataset was first clipped using the AIPS program CLIP well above the total found flux density found in the field from lower resolution observations in order to remove a few high points before beginning the self-calibration process.

2.2. Imaging & Self-calibration

The entire primary beam was then imaged using the AIPS task IMAGR and the 3D, multi-facet options. Besides 37 facets, each with 1000×1000 points, to describe the primary beam, another 37 facets, each with 500×500 points, were centered on all the remaining detectable sources outside of the central region. This is particularly important at 20cm since the feed is a compromise using a lens to illuminate the primary reflector. This feed causes both a higher system temperatures as a function of elevation and produces a high first sidelobe response for the primary beam. The result of this is that many outlying sources are detected in the first sidelobe, as well as a few further out which need to be removed. This was accomplished using the 37 outlying facets. After initial imaging, each detected source had a tight clean box placed around it to limit cleaning to real features. This procedure allows each image to cleaned down to the 1σ level and the resulting clean components to be used in the self calibration process. This process also eliminates almost all of the clean bias and does not artificially reduce the noise on the image as happens when one does not use boxes.

The images were self-calibrated, first just in phase, and later in both amplitude and phase using the AIPS task CALIB. However, these images were limited by the pointing changes on outlying bright sources. This is primarily due to the fact that the two circular polarizations have different pointing centers (*i.e.* beam squint) on the VLA due to the slightly off-axis location of the feeds. This combined with the alt-az geometry of the telescopes causes effective gain on a source far off-axis to vary with hour angle. Also the slightly different frequencies of the two IF's causes a slightly different primary beam size and thus a source far from the field center has an higher gain at the lower frequency. As a final step to correct approximately for these two effects, the uv datasets were split into their separate IF's (2), polarizations (2) and HA ranges (4). Then they were imaged and self-calibrated separately. Finally the eight images of each facet were combined, weighting each by $1/rms^2$ to form an optimum final image.

The final images had an *rms* noise, before correction for the primary beam, typically of 6.5 μJy, somewhat larger near very bright sources. The final full resolution images had a Gaussian clean beam with a FWHM of 1.60×1.52 arcseconds at a position angle of 87.9 degrees.

2.3. Cataloging

The inner 25×25 arcminute region of the final image was chosen for cataloging and further study. Beyond this region the losses due to the bandwidth smearing and the primary beam attenuation were judged to be too large for useful analysis. The AIPS program SAD was used for forming the initial source lists down to peak flux densities of 20 μJy/beam. The residual images from SAD were then searched to find any remaining sources sources missed by SAD. Lower resolution images with 3×3 arcseconds and 5×5 arcseconds were also constructed in order to search for lower surface brightness sources and to check the the fitted angular sizes for possible larger components than were detected on the full resolution images.

The full list of detected sources was then inspected and fitted manually using JMFIT. The parameter BWSMEAR was used to take into account the finite bandwidth of the individual 3.125 MHz channels used for the observing. Without using thus parameter, bandwidth smearing makes sources appear to be the (fractional bandwidth)$\times$(distance from the field center) in size, elongated radially from the phase pointing center. This results in typical apparent source sizes of a ~ 2 arcsec over the field analyzed and may account for some previous studies with the VLA for finding that typical size for sources in their samples. Sources which were found by JMFIT to have zero as the minimum size of the major axis were assumed to be unresolved. For such sources the maximum allowed size for the source on either axis was adopted as the upper limit to the angular extent. For unresolved sources, simulations have shown that the fitted peak flux density for the unconstrained, Gaussian functions fitted with JMFIT is the best estimate to the total flux density (Greisen 2002). Thus for sources with only upper limits to their size this estimate of the total flux density is used. For significantly resolved sources the total fitted flux density is adopted. Errors in the flux density and position were calculated using the formalism of Condon et al. (1998).

The local noise was estimated locally using the AIPS program, RMSD, in a 100×100 region centered on each pixel. This calculation was made on a mosaicked image of the entire 25×25 arcmin of the central field. The resulting noise image was then corrected for the primary beam attenuation, the bandwidth smearing and approximately for time averaging to produce a local noise image for the survey. This result was then used to pick source which had five sigma peaks in excess of the local noise on the full resolution image.

2.4. Optical Imaging

Optical and NIR images for the field were obtained of the same field in June 2000, using MOSAIC on the KPNO 4m and SQIID on the KPNO 2.1m. With MOSAIC, images were obtained in 8 bands: U, B, V, R, I, BATC 8010A, BATC 9170A, and WR CIII. The BATC filters (Fan et al 1996; Xia et al 2002) are special medium bandwidth filters ($\sim$ 250Å) designed to fit in the clearest optical windows in the red. WR CIII is a narrow-band filter centered at 4253Å with a FWHM of 52Å; we used it to isolate [OII] at the redshift of A2125. Total exposure times were U: 6 hours, B: 2 hours, V: 2 hours, R: 4 hours, I: 1 hour, 8010A: 2 hours, 9170A: 2 hours, WR CIII: 3.6 hours. The pointings were dithered to five separate pointing near the field center and then flattened and combined using the standard IRAF MOSAIC software as described by Valdes (2001). The standards of Landolt (1992) were used to set the magnitude scales on the UBVRI images. The USNO catalog of objects from the Palomar Sky Survey was used to set the astrometry on each final image. Each final image has a pixel size of 0.26 arcsec and is 8700×8800 pixels on a side.

2.5. Near IR Imaging

The SQIID images were taken simultaneously in J, H, and K. Each image has a usable field of $\sim 5.2 \times 5.2$ arcmin. Observations were obtained with SQIID over a 3x3 grid with 35” overlap across adjacent fields yielding a mosaicked field of view of 16.5 arcminutes. The mosaic consisted of 24 co-adds of 10 sec at each grid pointing. We applied random offsets between successive iterations of the mosaic. The total useful exposure time on the field was about 7 hours. More integration time was spend on the the central field and the field to to east of the center than on the other seven pointings.

As mosaicking a large area of sky with SQIID is not a standard observational mode, we summarize our data reduction method here. We first subtracted off a stacked dark exposure from all frames. For the sky subtraction we created a list of exposures over a ±30 minute window. Each frame was inspected and those with bright stars or higher than average background were removed. The dark-subtracted sky frame was then subtracted from all object frames in that time window. A master flatfield was created from all suitable exposures over the night and combined with sigma clipping and mode scaling. After flatfielding, we next removed any large-scale residual sky gradients by subtracting a median-filtered version of each frame. Next, each frame was corrected for geometrical distortion. The distortion map was determined separately for each filter based on a cross-correlation of objects with our deep R-band frame which had been previously re-gridded to a proper world coordinate system (distortions removed). Finally, we applied a bad-pixel mask to each frame which set bad regions to a very large positive number (100000) to facilitate threshold clipping during co-addition. Registering and stacking the data was accomplished by creating a zero-level image larger than the full field of the 3x3 grid (1800 pixels) and pasting each exposure into this image template. We used our R-band image (same image scale) as the reference image for determining pixel shifts. After measuring the shifts for each of the 9 frames in the grid, the frames were shifted and co-added with inverse-variance weighting and an upper threshold value set to clip off the bad regions set by the masking.

3. Results

Observations were taken of this field to study both the cluster and noncluster radio populations in the field of A2125. The cluster members were isolated using spectroscopic redshifts as reported in Miller et al (2004) and discussed in detail in Owen et al. (2004a). The remaining radio-detected objects are believed to predominately background sources. First, most have optical identifications much too faint to be cluster members and/or have spectroscopic redshifts outside the cluster limits. Second, as reported in Owen et al (2004b), our photometric redshift estimates or limits for very faint objects based on the implied absolute magnitudes for almost all the remaining objects are consistent with much higher redshifts than A2125 ($z = 0.247$). These sources and their parameters we list below. We will supply *fits* images of the radio and optical images on request.

3.1. Radio Catalog

In table 1, we give the final source list and parameters from the fits. Column (1) contains the source name. The first two digits are the facet number and the last three a sequence number. Columns (2) and (3) contain the radio RA and Dec along with the estimated error. In column (4) we give the distance from the pointing center (15 41 14.00, 66 15 00.0) in arcmin. Column (5) contains the observed (uncorrected) peak flux density from the map in μJy per beam. In column (6) we list the corrected total flux density and estimated error. In column (7), we give the best fit size in arcseconds. If a two dimensional Gaussian was the best fit, we give the major and minor axis size (FWHM) and the position angle. Upper limits are given for sources which were unresolved. Sources with sizes only were estimated directly from the maps using the AIPS task, TVSTAT. Column (8) contains the R-band optical magnitude in an aperture of radius 2 arcsec. Finally, column (9) gives the optical/NIR identification status. "i" indicates an identification in at least one of the 10 observed bands. "b" indicates a blank field. "c" indicates an optical field which is too confused to be sure of the identification. For the full sample of 357 radio sources 82% had a optical identification; 10% were confused; and 8% were blank and not confused.

3.2. Optical Identifications

Most of the sources in the radio catalog have clear identifications on the R-band image. For sources with apparent IDs within 1 arcsecond of the radio position, the mean radio-optical offset is -0.035 seconds of RA (-0.2 arcsec) and -0.1 arcsec in declination. After correcting for these offsets, the mean radio-optical separation is 0.3 arcsec. In figure 1 we show the histogram of the total radio-optical offset in arcseconds. Clearly most of the sources agree within a few tenths of an arcsec. However, both some of the radio and some of the optical sources are complex. Thus it seems prudent to catalog IDs out to offsets of at least one arcsec. In the few cases where sources appear much more extended than the beam, an attempt has been been made to assign an obvious ID. However, it is difficult to assess the reality of these IDs, statistically.

In figure 2 we show the histogram of optical magnitudes at R (within a two arcsecond radius aperture) for the identifications. The mean magnitude for the 257 objects with identifications in the R-band image is 22.6. The median magnitude is about 23.0 with some uncertainty due to the sources confused by very bright objects and objects not detected in R due to image imperfections.

In order to estimate the reliability of the IDs, SExtractor was run on the central 8×8

arcmin field of our R image, using an aperture of two arcsec radius. Since this field contains the central concentration of the cluster, the local source density should be somewhat higher than in the outlying fields. At a limiting magnitude of $R = 27.0$ (where we begin to be incomplete), we find 0.01 objects per square arcsec between 20.0 and 27.0. Down with a brighter limit of $R = 25.0$, we find 0.0016 objects per square degree. Given our 329 unconfused objects, we expect 10 false identifications down to 27.0. However, 77% of the objects have identifications brighter than 25.0. Since any objects fainter than 25.0 would be too faint to be designated the identification in the presence of a much brighter ID, we expect no more than one of these to be incorrect. Between 25.0 and 27.0 we might expect one false ID. Neither of these arguments take into account the full effect of the brighter identifications and thus this estimate is probably pessimistic. The argument does say that we expect a small number of cases where the correct identification will have a fainter confusing source within the one arcsec search area (and the seeing disk) as well.

4. Conclusion

We have presented the data reduction techniques and the catalog of radio detections of non-cluster members for the A2125 field. We also report the R-band optical identifications. We report the catalog of the detections for confirmed cluster members in a companion paper, as well as a more detailed interpretation of these results. Subsequent papers will report more detailed astrophysical results for this dataset.

REFERENCES

Carilli, C. L. & Yun, M. S. 1999, ApJ, 513, 13

Condon, J. J. 1992, A&A Rev., 30, 575

Condon, J. J., Cotton, W. D., Greisen, E. W., Yin, Q. F., Perley, R. A., Taylor, G. B., & Broderick, J. J., 1998, ApJ, 115, 1693

Dwarakanath, K. S. & Owen, F. N. 1999, AJ, 118, 625

Eales, S., Bertoldi, F., Ivison. R., Carilli, C., Dunne, L. & Owen, F. 2003, MNRAS, 344, 169

Fan, X., Burstein, D., Chen, J-S., Zhu, J., Jiang, Z., Wu, H., Yan, H., Zheng, Z., Zhou, X., Fang, L-Z., Chen, F., Deng, Z., Chu, Y., Hester, J. J., Windhorst, R. A., Li, Y., Lu, P., Sun, W-H., Chen, W-P., Tsay, W-S. Chiueh, T-H., Chou, C-K., Ko, C-M., Lin, T-C., Guo, H-J., & Byun, Y-I. 1996, AJ, 112, 628

Greisen, E. C. 2002, private communication

Landolt, A. U., AJ, 104, 340

Ledlow, M. J., Smail, I., Owen, F. N., Keel, W. C., Ivison, R. J., & Morrison, G. E., 2002, ApJ, 577, 79

Miller, N. A., Owen, F. N., Hill, J. M., Keel, W. C., Ledlow, M. J., & Oegerle, W. R. 2004, submitted

Owen, F. N., Ledlow, M. J., Keel, W. C., Wang, Q. D., & Morrison, G. E. 2004, in preparation

Owen, F. N., Dyer, K., Ledlow, M. J., Keel, W. C., & Wang, Q. D. 2004, in preparation

Owen, F. N., Ledlow, M. J., Keel, W. C., & Morrison, G. E, 1999, AJ, 118, 633

Valdes, F. G. 2001, in Automated Data Analysis in Astronomy, ed H. P. Singh and R. A. Gupta (http://iraf.noao.edu/projects/ccdmosaic/)

Wang, Q. D., Connolly, A. & Brunner, R. J. 1997, ApJ, 487, L13

Wang, Q. D., Owen, F. N., & Ledlow, M. J. 2004 submitted

Xia, L., Zhou, X., Ma, J., Wu, H., Sun, W-H., Jiang, Z., Xue, S., Chen, J., & Chen, W. 2002, PASP, 114, 1349

Yun, M. S., Reddy, N. A., & Condon, J. J. 2001, ApJ, 554, 803

This preprint was prepared with the AAS LaTeX macros v5.2.

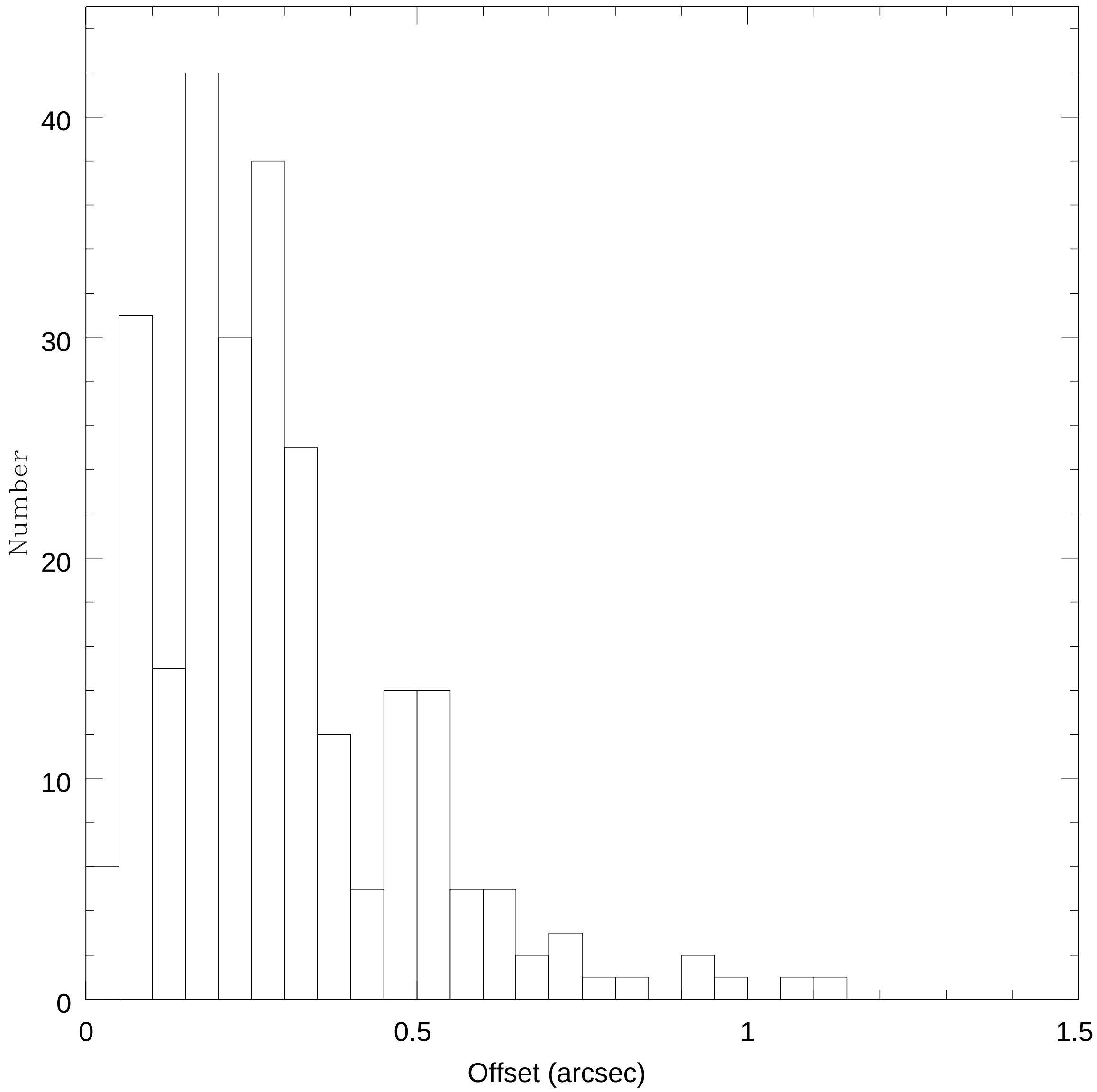

Fig. 1.— Histogram of the offsets between the positions of the radio sources and their optical identifications in arcsec.

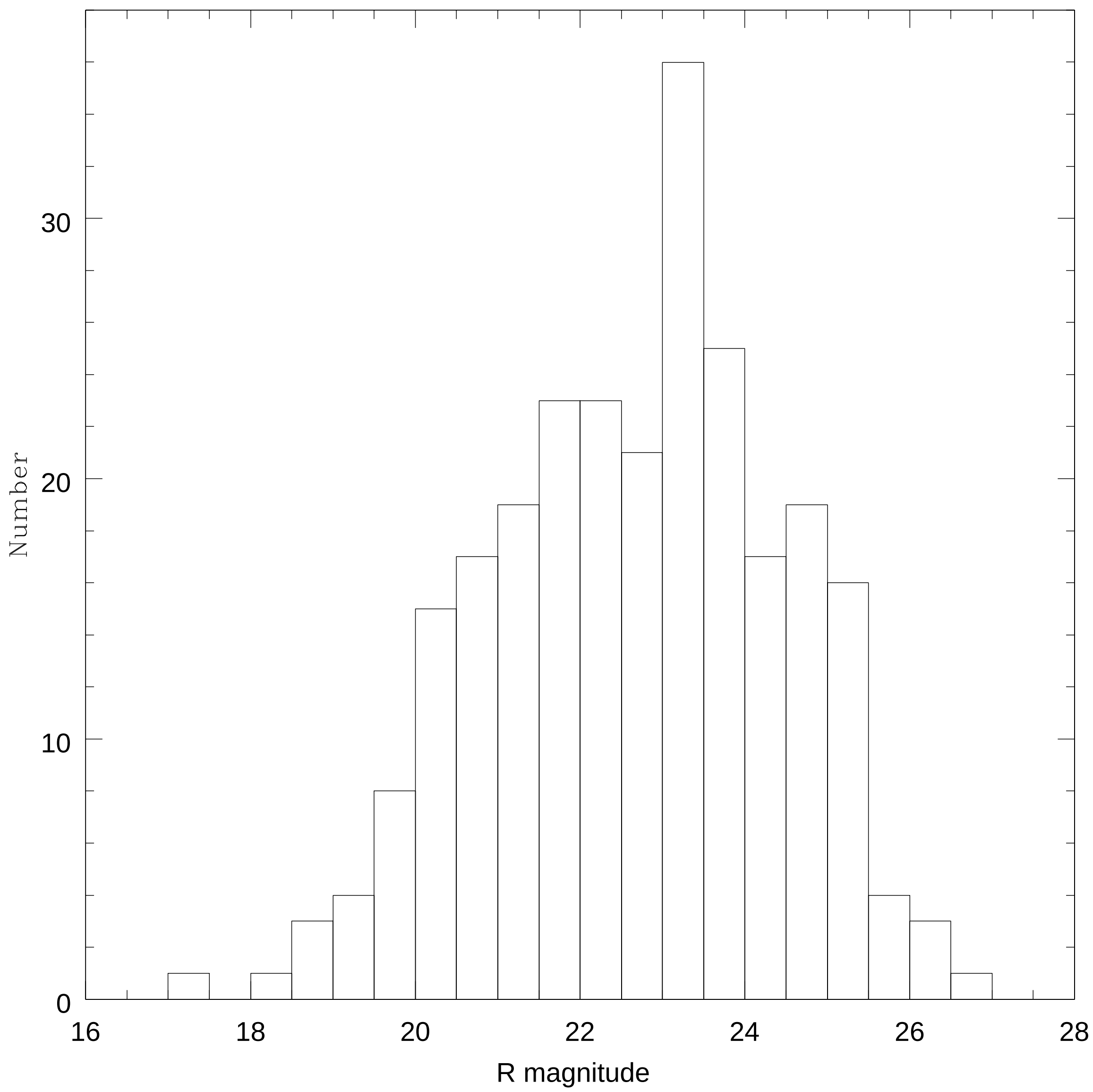

Fig. 2.— Histogram of R magnitudes of identifications in an aperture of two arcsec radius

Table 1. Non-cluster Member Radio Sources

Name	RA(2000.0)	Dec(2000.0)	Dist Mpc	Peak μJy/b	Total μJy	Size arcsec	Rmag	ID
18002	15 39 10.81(0.05)	66 14 58.3(0.3)	12.4	69.9	157.6(16.)	<1.7	22.44	i
11001	15 39 11.21(0.06)	66 19 45.9(0.4)	13.2	70.0	193.9(28.)	1.6x0p=118	0.00	b
11002	15 39 12.88(0.07)	66 25 10.1(0.4)	15.8	38.8	131.2(24.)	<1.2	23.48	i
18003	15 39 13.42(0.07)	66 12 15.7(0.4)	12.5	63.9	179.6(28.)	1.6x0.2p=71	24.42	i
11003	15 39 14.08(0.08)	66 22 20.2(0.5)	14.1	46.8	169.4(37.)	1.9x0.3p108	0.00	b
18004	15 39 15.80(0.07)	66 13 44.0(0.4)	12.0	57.5	175.7(31.)	2.0x0.8p=55	0.00	c
24001	15 39 16.18(0.04)	66 06 30.8(0.3)	14.6	136.2	420.7(27.)	0.7x0p=50	23.67	i
18005	15 39 16.24(0.07)	66 12 33.9(0.4)	12.1	37.8	77.9(15.)	<1.8	0.00	c
24002	15 39 16.97(0.07)	66 03 53.4(0.4)	16.3	38.1	133.6(25.)	<1.7	24.39	i
18006	15 39 17.05(0.03)	66 17 43.9(0.2)	12.1	267.0	645.8(29.)	1.2x0p=103	0.00	c
11005	15 39 17.35(0.08)	66 24 55.4(0.5)	15.3	43.7	238.6(60.)	2.8x0.9p=138	22.33	i
18007	15 39 17.45(0.07)	66 11 15.4(0.4)	12.3	56.2	170.8(29.)	1.7x0.5p=38	22.30	i
11006	15 39 17.49(0.05)	66 23 29.6(0.3)	14.4	110.9	382.0(34.)	1.4x0p=167	23.35	i
18008	15 39 17.62(0.03)	66 18 50.3(0.2)	12.3	352.1	854.3(32.)	0.9x0.1p=104	22.48	i
11007	15 39 18.11(0.07)	66 20 28.4(0.4)	12.9	55.8	182.7(32.)	1.8x0.6p=125	21.98	i
18009	15 39 18.62(0.07)	66 16 59.7(0.4)	11.8	44.3	89.0(14.)	<1.9	23.77	i
18010	15 39 19.69(0.08)	66 17 16.3(0.5)	11.7	42.1	110.7(27.)	1.8x0p=132	23.00	i
18011	15 39 20.06(0.07)	66 14 27.7(0.4)	11.5	43.2	87.9(14.)	<1.4	20.67	i
18012	15 39 21.57(0.06)	66 18 47.9(0.4)	11.9	48.8	103.9(15.)	<1.4	25.30	i
18015	15 39 22.80(0.07)	66 17 55.5(0.4)	11.6	42.8	87.8(15.)	<2.2	22.40	i
18016	15 39 24.04(0.09)	66 10 53.8(0.6)	11.8	35.4	88.8(28.)	2.0x0p=90	23.99	i
11008	15 39 25.19(0.07)	66 26 28.1(0.4)	15.8	43.3	145.1(24.)	<1.5	23.33	i
18017	15 39 26.08(0.07)	66 11 29.3(0.4)	11.4	39.5	76.6(14.)	<1.3	25.11	i
11009	15 39 26.16(0.08)	66 20 54.1(0.5)	12.3	33.3	73.9(16.)	<2.0	23.42	i
18019	15 39 31.14(0.04)	66 17 01.9(0.2)	10.5	183.1	337.6(16.)	<0.7	0.00	c
18020	15 39 32.04(0.07)	66 18 10.1(0.4)	10.7	40.1	75.2(13.)	<1.6	0.00	b
24004	15 39 33.09(0.05)	66 07 43.6(0.3)	12.5	176.4	817.8(59.)	4.5	20.55	i
24006	15 39 35.03(0.03)	66 08 03.8(0.2)	12.2	420.0	1134.6(51.)	3.5	0.00	i
18021	15 39 35.56(0.03)	66 14 56.7(0.2)	9.9	436.3	1341.8(61.)	25.0	23.72	i
18022	15 39 35.79(0.06)	66 11 26.3(0.4)	10.5	48.9	89.2(13.)	<1.7	19.80	i

Table 1—Continued

Name	RA(2000.0)	Dec(2000.0)	Dist Mpc	Peak μJy/b	Total μJy	Size arcsec	Rmag	ID
11010	15 39 36.00(0.07)	66 21 40.3(0.4)	11.9	35.7	75.1(15.)	<1.9	21.70	i
11102	15 39 38.07(0.10)	66 21 02.3(0.6)	11.4	33.6	120.9(47.)	5.2x0p=48	20.20	i
11011	15 39 39.05(0.07)	66 23 13.4(0.4)	12.6	44.9	101.4(16.)	<1.2	24.17	i
11012	15 39 39.46(0.04)	66 22 45.2(0.2)	12.2	140.6	306.0(18.)	<1.2	0.00	i
11013	15 39 41.14(0.04)	66 22 08.5(0.2)	11.7	153.2	315.7(17.)	<0.7	24.94	i
18024	15 39 41.89(0.06)	66 14 06.3(0.4)	9.3	58.3	95.2(12.)	<1.5	0.00	i
11014	15 39 42.55(0.08)	66 24 55.8(0.5)	13.5	45.7	169.8(43.)	2.7x0p=3	19.53	i
18025	15 39 42.72(0.08)	66 12 48.3(0.5)	9.5	33.5	55.3(12.)	<1.9	23.96	i
18026	15 39 43.46(0.07)	66 11 51.4(0.4)	9.7	39.4	66.0(12.)	<1.9	25.16	i
11015	15 39 44.30(0.09)	66 24 34.1(0.5)	13.1	47.4	133.1(35.)	2.5x0p=135	20.26	i
18027	15 39 45.42(0.02)	66 12 36.5(0.1)	9.2	1403.2	2312.5(70.)	0.5x0p=77	21.18	i
11016	15 39 46.16(0.07)	66 24 14.3(0.4)	12.8	39.4	90.2(16.)	<1.2	21.98	i
24009	15 39 46.28(0.06)	66 07 16.4(0.4)	11.8	55.2	112.2(15.)	<1.4	21.55	i
24010	15 39 47.06(0.02)	66 06 25.4(0.1)	12.3	14041.0	82465.0(2475.)	12.0	21.65	i
24011	15 39 46.41(0.07)	66 03 34.6(0.4)	14.5	61.5	300.5(51.)	2.6x0.9p=61	20.58	i
11017	15 39 46.43(0.08)	66 21 25.4(0.5)	10.9	40.8	114.1(26.)	1.8x0.7p=93	21.52	i
18028	15 39 49.35(0.06)	66 17 37.0(0.4)	8.9	58.3	91.7(11.)	<1.5	20.60	i
18029	15 39 50.53(0.05)	66 14 41.2(0.3)	8.4	97.4	146.6(11.)	<1.3	23.37	i
11019	15 39 50.58(0.07)	66 21 04.8(0.4)	10.3	41.3	73.7(13.)	<1.1	22.38	i
24013	15 39 50.95(0.06)	66 04 37.9(0.4)	13.4	54.0	129.5(17.)	<1.3	26.45	i
24014	15 39 51.04(0.06)	66 05 30.3(0.4)	12.7	74.3	277.5(40.)	2.5	22.49	i
11020	15 39 52.09(0.08)	66 20 00.2(0.5)	9.6	45.4	112.1(25.)	2.0x0p=57	22.98	i
24039	15 39 52.24(0.07)	66 07 15.6(0.4)	11.3	40.7	468.3(87.)	6.5x3.3p=178	0.00	c
18031	15 39 53.22(0.09)	66 18 32.8(0.5)	8.9	36.6	173.0(48.)	5.6	19.99	i
24017	15 39 53.25(0.04)	66 10 43.0(0.3)	9.2	114.5	182.7(12.)	<0.9	21.23	i
11021	15 39 53.82(0.06)	66 20 44.4(0.4)	9.9	47.4	80.8(12.)	<1.7	23.07	i
24018	15 39 54.54(0.02)	66 05 12.9(0.1)	12.7	4864.9	27202.0(818.)	2.8x1.6p=100	22.38	i
24019	15 39 55.74(0.07)	66 08 38.0(0.4)	10.2	43.7	75.5(12.)	<1.3	22.59	i
24020	15 39 56.01(0.08)	66 05 32.7(0.5)	12.3	43.9	190.2(46.)	3.1x1.0p=32	19.17	i
11022	15 39 56.94(0.05)	66 23 12.5(0.3)	11.3	94.5	183.5(15.)	<1.1	23.76	i

Table 1—Continued

Name	RA(2000.0)	Dec(2000.0)	Dist Mpc	Peak μJy/b	Total μJy	Size arcsec	Rmag	ID
11023	15 39 57.46(0.08)	66 24 29.6(0.5)	12.2	34.7	74.2(15.)	<1.6	21.31	i
11024	15 39 57.61(0.09)	66 24 41.5(0.5)	12.3	34.5	123.4(36.)	2.3x0.0p=25	21.68	i
18032	15 39 57.87(0.03)	66 13 31.6(0.2)	7.8	587.7	1152.6(46.)	6.1	0.00	c
24023	15 39 57.97(0.05)	66 07 49.4(0.3)	10.5	78.6	140.3(13.)	<1.5	25.06	i
24024	15 39 58.10(0.05)	66 03 17.4(0.3)	14.0	68.3	176.4(19.)	<1.4	23.75	i
18034	15 39 59.73(0.06)	66 17 04.0(0.3)	7.7	63.2	89.8(10.)	<1.3	25.17	i
24025	15 40 00.01(0.02)	66 05 51.6(0.1)	11.8	12640.0	26159.0(785.)	<0.3	20.93	i
11025	15 40 01.07(0.08)	66 22 16.7(0.5)	10.3	40.7	104.9(23.)	1.6x0.8p=4	23.23	i
11026	15 40 03.36(0.08)	66 22 22.6(0.5)	10.2	44.0	118.1(29.)	2.4x0p=172	21.15	i
11027	15 40 04.21(0.07)	66 25 23.4(0.4)	12.5	66.2	201.9(33.)	2.2x0p=86	22.05	i
18035	15 40 04.81(0.06)	66 13 48.7(0.3)	7.1	80.1	126.7(14.)	1.2x0p=163	21.00	i
18036	15 40 04.89(0.06)	66 13 02.9(0.4)	7.2	53.6	72.9(10.)	<0.9	0.00	b
24028	15 40 05.66(0.06)	66 07 20.1(0.3)	10.3	61.6	107.4(13.)	<1.8	23.75	i
24029	15 40 06.25(0.07)	66 09 41.5(0.4)	8.7	50.9	100.7(18.)	1.5x0.3p=59	25.14	i
24031	15 40 06.94(0.06)	66 02 50.6(0.4)	13.9	58.1	148.0(18.)	<1.7	23.09	i
18037	15 40 07.27(0.09)	66 15 59.9(0.5)	6.8	37.7	104.4(30.)	3.4x0p=44	0.00	c
18038	15 40 07.79(0.09)	66 17 13.4(0.6)	7.0	38.7	95.7(31.)	4.7x0p=127	21.80	i
18039	15 40 08.10(0.07)	66 16 25.5(0.4)	6.8	54.5	73.6(12.)	1.1x0p=33	21.90	i
18040	15 40 08.70(0.05)	66 15 36.2(0.3)	6.6	82.9	107.8(10.)	<0.7	20.06	i
11028	15 40 10.44(0.06)	66 24 38.5(0.4)	11.5	49.3	97.7(14.)	<2.0	23.26	i
11029	15 40 10.82(0.09)	66 19 22.3(0.5)	7.7	37.3	92.2(25.)	2.5x0p=89	21.46	i
11030	15 40 11.26(0.07)	66 23 06.2(0.4)	10.3	38.1	66.4(12.)	<1.2	21.57	i
24032	15 40 12.78(0.06)	66 03 21.5(0.4)	13.2	48.7	116.8(17.)	<2.1	0.00	c
18044	15 40 13.88(0.07)	66 18 29.4(0.4)	7.0	40.7	54.2(9.)	<1.2	0.00	c
18046	15 40 15.13(0.02)	66 18 13.1(0.1)	6.7	1064.3	1392.3(43.)	<0.3	23.11	i
18050	15 40 16.06(0.06)	66 16 28.6(0.4)	6.0	58.8	73.3(9.)	<0.8	0.00	c
11033	15 40 21.63(0.04)	66 24 15.1(0.2)	10.6	169.5	304.5(16.)	<1.0	22.62	i
18051	15 40 21.82(0.08)	66 17 54.9(0.5)	6.0	34.5	44.0(9.)	<1.1	0.00	i
18052	15 40 22.18(0.07)	66 18 35.0(0.4)	6.3	38.5	48.8(9.)	<1.7	0.00	c
24034	15 40 22.73(0.06)	66 06 30.3(0.4)	10.0	58.5	97.5(12.)	<1.7	25.45	i

Table 1—Continued

Name	RA(2000.0)	Dec(2000.0)	Dist Mpc	Peak μJy/b	Total μJy	Size arcsec	Rmag	ID
23035	15 40 22.93(0.06)	66 10 01.7(0.4)	7.2	55.0	73.2(10.)	<1.1	21.50	i
18053	15 40 23.44(0.07)	66 14 16.1(0.4)	5.1	45.4	53.4(8.)	<0.9	0.00	c
23036	15 40 24.60(0.06)	66 05 59.7(0.4)	10.3	50.9	87.7(12.)	<1.8	21.51	i
11034	15 40 24.75(0.06)	66 19 19.9(0.3)	6.6	64.4	82.8(9.)	<0.8	22.68	i
18054	15 40 25.41(0.06)	66 16 14.2(0.4)	5.0	52.9	61.9(8.)	<0.9	0.00	i
18055	15 40 26.53(0.08)	66 15 30.3(0.5)	4.8	41.6	60.7(13.)	1.4x0p=90	20.81	i
24037	15 40 28.37(0.07)	66 03 53.5(0.4)	12.0	43.2	88.2(15.)	<1.8	20.95	i
11035	15 40 29.16(0.08)	66 20 07.6(0.5)	6.8	34.0	44.3(9.)	<2.5	21.63	i
11036	15 40 29.39(0.07)	66 22 26.3(0.4)	8.7	75.7	139.0(21.)	2.2x0p=66	0.00	b
11037	15 40 29.54(0.08)	66 24 10.0(0.5)	10.2	33.2	56.9(12.)	<1.7	21.24	i
18058	15 40 30.23(0.05)	66 17 19.6(0.3)	5.0	76.3	88.8(9.)	<0.9	0.00	i
18059	15 40 30.46(0.07)	66 15 30.9(0.4)	4.4	47.2	58.2(11.)	1.2x0p=133	23.77	i
18063	15 40 31.60(0.07)	66 17 10.8(0.4)	4.8	39.8	45.8(8.)	<1.6	21.69	i
12200	15 40 33.55(0.07)	66 22 31.1(0.4)	8.5	33.0	56.4(11.)	<1.4	23.26	i
25002	15 40 33.60(0.03)	66 08 01.3(0.2)	8.1	516.0	860.9(29.)	0.8x0.5p=12	21.20	i
25003	15 40 33.80(0.05)	66 07 24.3(0.3)	8.6	86.1	127.3(11.)	<1.3	20.42	i
12001	15 40 33.91(0.07)	66 20 03.8(0.4)	6.5	46.5	59.1(9.)	<1.6	25.18	i
00003	15 40 35.24(0.05)	66 12 04.6(0.3)	4.9	84.8	97.6(9.)	<1.0	21.84	i
00004	15 40 35.56(0.03)	66 16 56.6(0.2)	4.3	407.3	457.6(16.)	<0.5	23.80	i
12002	15 40 36.18(0.06)	66 20 46.9(0.4)	6.9	48.9	64.0(9.)	<1.0	0.00	b
00005	15 40 36.74(0.04)	66 15 41.4(0.2)	3.8	181.9	199.5(10.)	<0.7	22.93	i
25005	15 40 37.75(0.06)	66 07 48.3(0.4)	8.1	57.4	81.1(10.)	<1.7	21.16	i
25006	15 40 37.75(0.07)	66 08 23.4(0.4)	7.6	69.3	168.9(30.)	3.8x0p=154	21.24	i
00006	15 40 37.85(0.07)	66 12 32.7(0.4)	4.4	38.7	43.3(8.)	<0.9	0.00	b
12003	15 40 38.03(0.07)	66 20 18.4(0.4)	6.4	35.7	45.2(9.)	<1.2	22.06	i
25007	15 40 38.47(0.07)	66 08 33.3(0.4)	7.4	43.8	58.8(10.)	<1.3	23.46	i
25008	15 40 40.06(0.03)	66 06 30.6(0.2)	9.2	517.7	799.7(26.)	<0.4	23.61	i
12005	15 40 40.22(0.05)	66 21 09.3(0.3)	7.0	101.1	132.9(10.)	<1.0	24.50	i
12069	15 40 40.79(0.05)	66 26 54.1(0.3)	12.4	79.8	1848.0(150.)	20.0	17.40	i
12006	15 40 41.24(0.05)	66 25 25.6(0.3)	10.9	88.7	162.3(14.)	<1.1	24.32	i

Table 1—Continued

Name	RA(2000.0)	Dec(2000.0)	Dist Mpc	Peak μJy/b	Total μJy	Size arcsec	Rmag	ID
25009	15 40 42.55(0.03)	66 08 54.1(0.2)	6.9	320.8	414.8(15.)	<0.5	20.87	i
00009	15 40 44.24(0.07)	66 16 54.2(0.4)	3.5	43.6	55.4(11.)	1.2x0p=147	21.86	i
25012	15 40 44.91(0.02)	66 09 04.8(0.1)	6.6	36362.0	46134.0(1384.)	<0.1	22.09	i
12009	15 40 45.81(0.09)	66 23 31.9(0.5)	9.0	37.1	82.7(25.)	2.4x0p=74	22.62	i
12010	15 40 46.43(0.07)	66 21 01.6(0.4)	6.6	47.0	59.9(9.)	<1.2	23.81	i
12011	15 40 46.44(0.05)	66 26 19.4(0.3)	11.7	94.2	185.1(15.)	<1.1	24.06	i
00011	15 40 47.19(0.05)	66 15 51.8(0.3)	2.8	102.2	107.7(8.)	<1.0	24.51	i
00012	15 40 47.32(0.07)	66 11 37.9(0.4)	4.3	39.0	43.4(8.)	<1.2	22.65	i
00013	15 40 47.61(0.09)	66 12 08.7(0.5)	3.9	36.4	43.1(12.)	1.6x0p=119	24.82	i
12012	15 40 47.78(0.07)	66 20 56.2(0.4)	6.5	45.1	56.8(9.)	<1.0	23.14	i
12013	15 40 48.13(0.04)	66 24 02.7(0.3)	9.4	121.2	191.9(12.)	<0.7	21.95	i
12014	15 40 48.42(0.05)	66 22 58.6(0.3)	8.4	68.6	99.5(11.)	<0.9	22.79	i
12015	15 40 48.99(0.09)	66 20 24.2(0.5)	6.0	36.2	56.2(15.)	1.7x0p=0	24.92	i
12016	15 40 49.87(0.07)	66 20 15.1(0.4)	5.8	53.7	200.3(40.)	8.0x0p=9	0.00	c
12017	15 40 49.57(0.06)	66 21 05.5(0.4)	6.6	56.1	71.2(9.)	<1.2	21.74	i
00016	15 40 50.13(0.06)	66 16 40.2(0.4)	2.9	54.4	75.4(11.)	1.1x0.5p=90	0.00	c
00015	15 40 50.15(0.04)	66 10 45.7(0.2)	4.9	176.1	236.1(13.)	1.0x0p=140	21.89	i
00017	15 40 50.44(0.02)	66 10 55.4(0.1)	4.7	4413.5	11876.0(357.)	2.8x1.1p=13	22.17	i
00018	15 40 50.51(0.07)	66 13 01.0(0.4)	3.1	40.7	43.1(8.)	<0.9	21.77	i
00019	15 40 50.98(0.06)	66 16 32.3(0.3)	2.8	84.4	89.9(10.)	1.0x0p=7	18.80	i
25014	15 40 51.79(0.03)	66 06 30.9(0.2)	8.8	256.8	383.0(16.)	<0.6	19.28	i
00021	15 40 52.60(0.06)	66 16 36.6(0.4)	2.7	52.3	54.7(8.)	<1.1	24.96	i
00023	15 40 53.00(0.09)	66 16 54.4(0.5)	2.8	37.2	40.2(12.)	1.6x0p=51	23.35	i
00024	15 40 53.31(0.08)	66 19 01.5(0.5)	4.5	46.8	95.6(19.)	2.2	0.00	c
12020	15 40 54.24(0.05)	66 21 31.7(0.3)	6.8	69.1	89.1(9.)	<1.4	20.12	i
00025	15 40 54.43(0.07)	66 12 50.3(0.4)	2.9	47.0	49.4(8.)	<1.0	22.71	i
12021	15 40 54.68(0.08)	66 20 48.5(0.5)	6.1	40.0	74.8(18.)	1.9x0.1p=137	0.00	i
12022	15 40 54.91(0.07)	66 20 43.8(0.4)	6.0	47.3	57.9(9.)	<1.7	22.71	i
12023	15 40 55.29(0.03)	66 21 52.0(0.2)	7.1	290.2	426.5(17.)	0.7x0.4p=52	22.77	i
12024	15 40 55.51(0.06)	66 25 19.1(0.4)	10.5	47.7	83.2(12.)	<1.3	24.15	i

Table 1—Continued

Name	RA(2000.0)	Dec(2000.0)	Dist Mpc	Peak μJy/b	Total μJy	Size arcsec	Rmag	ID
12025	15 40 55.87(0.07)	66 27 09.3(0.4)	12.3	42.8	89.7(15.)	<1.4	23.38	i
00029	15 40 56.37(0.06)	66 16 28.2(0.4)	2.3	52.0	53.7(7.)	<0.8	22.36	i
12026	15 40 56.72(0.10)	66 24 24.5(0.6)	9.6	36.0	114.5(40.)	5.8x1.8p=7	0.00	i
12071	15 40 56.73(0.09)	66 26 25.2(0.5)	11.5	36.4	98.9(30.)	2.3x0p=36	23.23	i
00030	15 40 56.88(0.05)	66 17 26.5(0.3)	3.0	91.4	128.6(12.)	1.1x0.6p=33	23.15	i
25016	15 40 57.38(0.04)	66 06 39.2(0.3)	8.5	122.2	178.2(12.)	<1.1	24.52	i
12028	15 40 59.42(0.07)	66 20 27.4(0.4)	5.6	51.3	78.7(15.)	1.6x0p=71	25.21	i
00032	15 40 59.59(0.07)	66 12 16.4(0.4)	3.1	49.2	83.6(16.)	1.9x0.2p=56	22.10	i
00033	15 41 00.63(0.06)	66 13 53.9(0.4)	1.7	85.8	185.8(28.)	6.7	21.29	i
00035	15 41 00.85(0.04)	66 18 00.4(0.2)	3.3	133.3	142.0(9.)	<0.7	25.18	i
12030	15 41 00.85(0.06)	66 24 52.7(0.3)	10.0	62.8	104.3(12.)	<1.2	0.00	i
00037	15 41 01.06(0.05)	66 14 16.3(0.3)	1.5	81.0	113.3(11.)	1.1x0.8p=13	0.00	b
00038	15 41 01.52(0.07)	66 13 54.2(0.4)	1.7	42.2	42.9(7.)	<1.3	20.61	i
25018	15 41 02.03(0.02)	66 07 11.5(0.1)	7.9	711.0	986.8(31.)	<0.3	23.01	i
00040	15 41 02.19(0.07)	66 18 15.0(0.4)	3.5	38.4	41.1(8.)	<1.2	0.00	i
00041	15 41 02.89(0.07)	66 13 05.7(0.4)	2.2	44.2	44.4(7.)	<1.0	0.00	c
12031	15 41 03.07(0.07)	66 26 31.1(0.4)	11.6	45.3	87.8(14.)	<1.8	22.22	i
00042	15 41 04.65(0.05)	66 14 56.4(0.3)	0.9	68.9	69.3(7.)	<1.2	24.23	i
00043	15 41 05.35(0.06)	66 12 35.6(0.4)	2.6	64.2	124.9(18.)	2.1x0.8p=53	19.27	i
12032	15 41 06.38(0.06)	66 23 33.3(0.4)	8.6	55.7	81.7(11.)	<1.4	0.00	i
12034	15 41 07.31(0.04)	66 21 23.7(0.2)	6.4	161.6	202.0(11.)	<1.2	21.35	i
12035	15 41 07.45(0.06)	66 23 35.5(0.4)	8.6	57.7	84.6(11.)	<1.6	0.00	c
00044	15 41 07.61(0.07)	66 16 56.8(0.4)	2.0	44.9	46.0(7.)	<1.4	20.84	i
00045	15 41 09.25(0.07)	66 14 43.8(0.4)	0.5	42.7	42.8(7.)	<1.4	0.00	i
25020	15 41 09.39(0.06)	66 08 07.3(0.4)	6.9	72.7	105.1(13.)	1.1x0p=2	23.80	i
12037	15 41 09.72(0.05)	66 23 25.7(0.3)	8.4	81.1	117.7(11.)	<0.8	0.00	c
00048	15 41 09.91(0.07)	66 10 58.7(0.4)	4.0	39.5	43.2(8.)	<1.7	23.93	i
12038	15 41 10.04(0.06)	66 22 10.5(0.4)	7.2	57.3	75.5(9.)	<1.3	0.00	c
12039	15 41 10.55(0.07)	66 21 44.7(0.4)	6.8	38.5	49.2(9.)	<1.5	0.00	i
00049	15 41 10.63(0.05)	66 13 13.9(0.3)	1.8	104.0	105.9(8.)	<0.9	20.34	i

Table 1—Continued

Name	RA(2000.0)	Dec(2000.0)	Dist Mpc	Peak μJy/b	Total μJy	Size arcsec	Rmag	ID
00050	15 41 10.75(0.07)	66 12 09.7(0.4)	2.9	37.6	39.4(7.)	<1.5	22.25	i
12040	15 41 10.95(0.07)	66 27 07.8(0.4)	12.1	60.9	126.1(23.)	1.7x0p=4	0.00	b
12041	15 41 11.08(0.07)	66 24 35.8(0.4)	9.6	53.1	129.2(22.)	1.7x0.4p=107	24.54	i
00053	15 41 12.47(0.06)	66 17 16.7(0.4)	2.3	55.9	57.6(7.)	<1.5	21.67	i
00054	15 41 12.87(0.07)	66 15 02.0(0.4)	0.1	37.0	37.0(7.)	<0.9	21.71	i
00055	15 41 13.51(0.07)	66 13 03.9(0.4)	1.9	41.6	42.5(7.)	<0.9	23.48	i
25107	15 41 13.87(0.07)	66 09 02.2(0.4)	6.0	37.7	50.7(9.)	<1.0	0.00	b
00058	15 41 14.78(0.04)	66 13 30.7(0.2)	1.5	134.6	136.4(8.)	<0.7	0.00	i
12043	15 41 15.31(0.06)	66 25 29.1(0.3)	10.5	63.3	110.0(13.)	<1.1	23.09	i
12044	15 41 16.91(0.06)	66 26 16.1(0.4)	11.3	60.8	166.4(23.)	1.3x1.0p=8	23.50	i
00061	15 41 16.97(0.06)	66 16 26.7(0.3)	1.5	74.8	188.1(22.)	2.5x1.2p=90	20.80	i
12045	15 41 17.85(0.05)	66 22 33.7(0.3)	7.6	104.2	141.0(10.)	<0.7	0.00	c
25023	15 41 20.72(0.07)	66 09 33.5(0.4)	5.5	38.4	46.2(9.)	<1.8	24.99	i
12046	15 41 20.80(0.08)	66 19 20.7(0.5)	4.4	40.4	140.3(33.)	4.3x2.0p=48	19.88	i
00063	15 41 22.47(0.05)	66 18 58.0(0.3)	4.1	72.5	79.5(8.)	<1.3	0.00	b
12048	15 41 23.73(0.05)	66 20 35.8(0.3)	5.7	86.6	103.3(9.)	<1.3	0.00	b
00064	15 41 24.03(0.06)	66 16 14.9(0.4)	1.6	66.2	369.0(48.)	24.0	22.96	i
12049	15 41 24.16(0.06)	66 22 11.1(0.3)	7.3	67.6	89.4(10.)	<0.8	22.03	i
00065	15 41 24.23(0.08)	66 16 40.0(0.5)	2.0	40.3	87.2(19.)	2.3x0.8p=95	0.00	b
00066	15 41 24.26(0.05)	66 12 21.6(0.3)	2.8	105.8	110.8(8.)	<1.0	22.87	i
25024	15 41 24.26(0.07)	66 07 56.7(0.4)	7.1	42.7	56.1(9.)	<1.4	21.30	i
25025	15 41 24.44(0.04)	66 09 03.0(0.2)	6.0	135.2	165.0(10.)	<0.8	0.00	i
25026	15 41 24.91(0.05)	66 05 25.6(0.3)	9.6	81.2	130.6(12.)	<1.4	22.64	i
00067	15 41 25.49(0.07)	66 14 41.8(0.4)	1.2	46.9	47.3(7.)	<1.4	0.00	i
12050	15 41 26.06(0.04)	66 20 57.1(0.2)	6.1	139.9	170.8(10.)	<1.0	0.00	i
00068	15 41 26.16(0.07)	66 13 41.4(0.4)	1.8	37.2	38.0(7.)	<1.4	0.00	b
12051	15 41 26.62(0.06)	66 27 21.5(0.4)	12.4	75.8	172.4(21.)	1.2x0p=5	24.17	i
25027	15 41 26.82(0.07)	66 02 54.1(0.4)	12.2	54.1	143.9(27.)	1.8x0.2p=179	23.75	i
00069	15 41 26.90(0.06)	66 14 37.3(0.3)	1.4	82.0	86.4(10.)	1.1x0p=8	0.00	b
25028	15 41 27.28(0.07)	66 04 53.4(0.4)	10.2	43.9	74.4(12.)	<1.8	23.35	i

Table 1—Continued

Name	RA(2000.0)	Dec(2000.0)	Dist Mpc	Peak μJy/b	Total μJy	Size arcsec	Rmag	ID
00071	15 41 27.29(0.06)	66 16 17.0(0.3)	1.9	63.4	67.0(8.)	<1.1	0.00	b
00072	15 41 27.37(0.06)	66 17 40.9(0.4)	3.0	57.3	83.4(12.)	1.3x0.6p=158	23.02	i
00073	15 41 27.66(0.06)	66 17 08.8(0.4)	2.5	55.6	57.8(7.)	<1.3	24.74	i
00074	15 41 27.66(0.07)	66 15 34.2(0.4)	1.5	37.7	38.2(7.)	<1.0	25.32	i
25029	15 41 27.89(0.06)	66 07 58.8(0.4)	7.2	54.6	71.9(9.)	<1.6	23.27	i
00075	15 41 28.07(0.04)	66 13 26.1(0.3)	2.1	89.0	1318.0(86.)	18.0	18.23	i
25030	15 41 28.12(0.07)	66 05 16.6(0.4)	9.8	40.7	66.6(12.)	<1.9	2.90	i
12052	15 41 28.27(0.04)	66 22 55.4(0.3)	8.1	107.1	150.5(11.)	<0.9	23.56	i
00076	15 41 28.55(0.08)	66 16 01.6(0.5)	1.8	41.9	76.2(17.)	2.0x0.8p=15	21.96	i
12053	15 41 28.78(0.02)	66 22 02.7(0.1)	7.2	1004.4	1323.3(41.)	0.4x0p=9	24.26	i
12054	15 41 29.02(0.02)	66 22 10.0(0.1)	7.3	744.1	989.2(31.)	0.3x0p=9	0.00	b
25032	15 41 29.75(0.09)	66 04 51.5(0.5)	10.3	38.8	109.6(32.)	2.9x0p=94	21.22	i
25033	15 41 29.78(0.08)	66 10 02.8(0.5)	5.2	39.4	71.4(16.)	1.6x0.7p=36	0.00	b
12108	15 41 30.62(0.07)	66 25 39.0(0.4)	10.8	36.6	65.4(13.)	<1.7	23.67	i
12055	15 41 31.12(0.06)	66 22 55.4(0.3)	8.1	60.1	84.8(10.)	<1.2	0.00	i
25035	15 41 31.56(0.07)	66 05 11.0(0.4)	10.0	38.5	63.9(12.)	<1.1	23.76	c
12056	15 41 31.88(0.07)	66 20 22.9(0.4)	5.7	50.3	76.7(15.)	1.6x0p=67	25.09	i
12057	15 41 33.21(0.07)	66 19 53.1(0.4)	5.3	43.3	50.5(8.)	<1.0	0.00	i
00079	15 41 33.21(0.06)	66 11 57.7(0.4)	3.6	49.1	53.0(8.)	<1.2	0.00	c
25036	15 41 33.29(0.07)	66 08 33.3(0.4)	6.7	44.4	56.8(9.)	<1.5	21.37	i
25037	15 41 33.42(0.06)	66 09 36.2(0.4)	5.7	54.6	65.6(9.)	<1.3	22.60	i
00080	15 41 33.58(0.07)	66 13 31.3(0.4)	2.5	39.7	41.2(7.)	<1.7	0.00	c
00081	15 41 35.63(0.06)	66 15 04.6(0.3)	2.2	74.1	105.4(13.)	1.4x0.3p=118	0.00	i
00082	15 41 36.51(0.07)	66 16 50.5(0.4)	2.9	42.5	44.7(7.)	<1.2	25.07	i
25040	15 41 39.95(0.06)	66 03 05.4(0.4)	12.2	52.8	109.9(15.)	<1.7	20.36	i
12059	15 41 41.01(0.02)	66 22 37.9(0.1)	8.1	37676.0	57741.0(1732.)	20.0	20.67	i
00086	15 41 41.75(0.07)	66 15 02.8(0.4)	2.8	54.1	96.1(17.)	2.0	0.00	i
00087	15 41 41.92(0.04)	66 11 10.3(0.2)	4.8	149.0	170.0(9.)	<0.6	24.74	i
25041	15 41 42.46(0.06)	66 06 22.4(0.4)	9.1	48.9	75.4(11.)	<1.4	24.42	i
25042	15 41 42.79(0.05)	66 06 46.8(0.3)	8.7	69.4	103.7(11.)	<1.5	23.45	i

Table 1—Continued

Name	RA(2000.0)	Dec(2000.0)	Dist Mpc	Peak μJy/b	Total μJy	Size arcsec	Rmag	ID
25043	15 41 42.93(0.06)	66 05 58.2(0.4)	9.5	55.8	89.2(12.)	<1.8	23.98	i
25044	15 41 43.34(0.07)	66 04 33.5(0.4)	10.9	61.6	140.4(27.)	2.3x0p=165	23.24	i
12060	15 41 43.76(0.07)	66 25 17.4(0.4)	10.7	52.7	143.1(26.)	1.9x0.8p=27	23.47	i
00090	15 41 44.84(0.07)	66 13 48.3(0.4)	3.3	38.5	41.3(8.)	<1.7	21.33	i
00091	15 41 45.03(0.05)	66 15 11.3(0.3)	3.1	88.9	94.7(8.)	<1.1	23.52	i
00092	15 41 45.29(0.08)	66 13 57.0(0.5)	3.3	45.5	52.7(11.)	1.4x0p=51	24.32	i
00093	15 41 46.18(0.06)	66 13 53.9(0.4)	3.4	57.6	62.1(8.)	<1.1	22.39	i
00094	15 41 46.24(0.07)	66 11 15.7(0.4)	5.0	39.1	45.1(8.)	<1.2	20.48	i
00095	15 41 47.26(0.07)	66 17 08.6(0.4)	4.0	39.3	43.2(8.)	<1.6	20.27	i
00096	15 41 47.36(0.09)	66 11 25.4(0.5)	4.9	42.5	140.0(37.)	9.0	0.00	i
00097	15 41 48.80(0.03)	66 11 36.8(0.2)	4.9	330.4	2112.0(83.)	37.0	0.00	i
12062	15 41 49.65(0.06)	66 25 54.2(0.4)	11.5	58.5	112.4(14.)	<1.5	22.47	i
25045	15 41 50.24(0.07)	66 05 32.4(0.4)	10.1	45.7	77.6(12.)	<1.4	24.86	i
00100	15 41 51.57(0.06)	66 16 43.1(0.4)	4.2	49.4	55.0(8.)	<1.1	25.14	i
12063	15 41 52.56(0.06)	66 27 25.9(0.4)	13.0	48.6	110.3(16.)	<1.8	21.32	i
25046	15 41 52.73(0.06)	66 05 29.3(0.4)	10.3	52.3	90.2(12.)	<1.3	24.20	i
12064	15 41 53.72(0.04)	66 20 30.7(0.2)	6.8	244.7	1132.3(59.)	18.0	0.00	c
12066	15 41 54.39(0.03)	66 23 23.0(0.2)	9.3	316.4	496.4(19.)	<0.5	0.00	c
00102	15 41 54.56(0.05)	66 16 24.0(0.3)	4.3	69.9	78.5(8.)	<1.2	22.61	i
00103	15 41 54.73(0.09)	66 15 52.9(0.5)	4.2	39.2	75.6(22.)	3.0x1.1p=76	23.90	i
19001	15 41 56.96(0.03)	66 12 10.9(0.2)	5.2	320.4	376.7(14.)	<0.7	23.01	i
19002	15 41 57.34(0.06)	66 13 22.2(0.4)	4.7	54.3	62.2(8.)	<0.8	0.00	c
19003	15 41 57.43(0.09)	66 12 56.3(0.5)	4.8	37.6	49.2(13.)	1.5x0p=75	19.95	i
19005	15 41 58.27(0.07)	66 13 11.9(0.4)	4.8	45.7	52.8(8.)	<1.0	25.84	i
13001	15 41 59.29(0.06)	66 23 26.3(0.3)	9.6	61.1	98.5(12.)	<1.3	23.47	i
19006	15 42 00.00(0.07)	66 18 43.0(0.4)	5.9	50.5	96.4(16.)	1.5x0.8p=119	22.82	i
19007	15 42 00.60(0.07)	66 18 09.3(0.4)	5.6	43.8	52.5(9.)	<1.4	0.00	b
26004	15 42 01.11(0.08)	66 10 11.4(0.5)	6.8	38.3	58.8(15.)	1.6x0p=67	20.21	i
19009	15 42 01.41(0.05)	66 14 31.1(0.3)	4.8	71.9	83.1(8.)	<1.2	0.00	i
19010	15 42 02.18(0.02)	66 13 00.5(0.1)	5.2	5618.7	13249.0(399.)	8.6	25.00	i

Table 1—Continued

Name	RA(2000.0)	Dec(2000.0)	Dist Mpc	Peak μJy/b	Total μJy	Size arcsec	Rmag	ID
26005	15 42 02.48(0.07)	66 06 46.8(0.4)	9.6	47.2	76.6(12.)	<2.0	22.09	i
13002	15 42 03.07(0.07)	66 20 15.2(0.4)	7.2	47.0	62.8(10.)	<1.7	0.00	c
19012	15 42 03.38(0.02)	66 17 40.2(0.1)	5.6	2320.5	2804.0(85.)	<0.2	26.02	i
19013	15 42 03.45(0.05)	66 15 53.3(0.3)	5.1	102.4	119.9(9.)	<1.1	0.00	c
19014	15 42 05.59(0.05)	66 15 27.7(0.3)	5.2	102.9	121.8(9.)	<1.1	0.00	c
19015	15 42 05.86(0.07)	66 13 30.9(0.4)	5.4	35.4	41.9(8.)	<1.3	23.71	i
19016	15 42 05.88(0.06)	66 16 52.7(0.3)	5.5	63.0	75.9(9.)	<1.3	22.55	i
13106	15 42 06.70(0.09)	66 19 11.6(0.5)	6.8	37.1	107.1(31.)	3.9x2.0p=102	22.14	i
19019	15 42 07.53(0.02)	66 19 00.6(0.1)	6.7	2442.4	3562.1(108.)	1.0x0p=136	24.18	i
19020	15 42 08.22(0.02)	66 18 42.9(0.1)	6.6	1246.6	1602.9(49.)	<0.4	24.94	i
26007	15 42 08.74(0.05)	66 06 02.1(0.3)	10.5	72.4	128.8(13.)	<1.5	23.72	i
19021	15 42 09.19(0.05)	66 13 49.4(0.3)	5.7	82.4	105.3(11.)	0.9x0p=161	26.07	i
19022	15 42 09.77(0.09)	66 14 51.4(0.5)	5.6	47.8	81.4(22.)	3.4x0p=45	20.65	i
19023	15 42 10.11(0.06)	66 12 17.1(0.4)	6.3	47.8	60.5(9.)	<1.4	23.62	i
13005	15 42 10.72(0.05)	66 21 13.8(0.3)	8.4	113.6	174.6(14.)	1.0x0p=172	0.00	b
19024	15 42 10.87(0.08)	66 11 09.9(0.5)	6.9	45.8	94.8(22.)	2.4 lrms=6.8	0.00	b
13006	15 42 11.08(0.05)	66 25 13.9(0.3)	11.7	135.2	327.8(24.)	1.4x0.4p=43	24.96	i
19025	15 42 11.09(0.07)	66 12 07.8(0.4)	6.4	40.3	50.9(9.)	<1.5	0.00	b
26008	15 42 11.39(0.06)	66 04 36.5(0.3)	11.9	66.0	135.0(15.)	<1.6	20.33	i
13007	15 42 11.54(0.06)	66 25 43.6(0.3)	12.2	62.0	129.2(15.)	<2.1	25.72	i
26009	15 42 11.87(0.07)	66 05 41.7(0.4)	11.0	39.9	74.4(13.)	<1.1	25.56	i
19026	15 42 13.03(0.08)	66 13 26.5(0.5)	6.2	34.3	43.1(9.)	<1.8	0.00	i
19027	15 42 14.76(0.06)	66 17 07.7(0.3)	6.5	80.1	105.2(11.)	0.9x0p=53	20.78	i
13010	15 42 14.82(0.03)	66 22 49.6(0.2)	9.9	271.8	455.1(18.)	<0.7	0.00	i
26011	15 42 15.09(0.05)	66 10 17.3(0.3)	7.8	73.6	103.7(10.)	<1.0	0.00	b
19028	15 42 15.37(0.07)	66 18 09.7(0.4)	6.9	47.2	104.2(18.)	1.5x1.2p=165	0.00	b
19029	15 42 15.39(0.05)	66 17 53.1(0.3)	6.8	82.7	108.5(10.)	<1.1	23.41	i
19030	15 42 15.54(0.07)	66 16 41.5(0.4)	6.4	47.1	60.3(9.)	<1.0	23.49	i
13035	15 42 15.94(0.07)	66 19 52.7(0.4)	7.9	44.0	62.3(10.)	<1.3	0.00	c
19031	15 42 16.00(0.08)	66 14 44.1(0.5)	6.2	45.8	70.3(14.)	1.4x0p=20	23.36	i

Table 1—Continued

Name	RA(2000.0)	Dec(2000.0)	Dist Mpc	Peak μJy/b	Total μJy	Size arcsec	Rmag	ID
13011	15 42 16.40(0.02)	66 19 33.0(0.1)	7.7	3558.2	23352.0(703.)	15.0	22.27	i
19032	15 42 16.91(0.07)	66 15 28.2(0.4)	6.3	47.1	60.1(9.)	<1.3	0.00	i
19033	15 42 17.51(0.06)	66 12 02.7(0.3)	7.1	67.7	90.8(10.)	<1.0	23.16	i
26012	15 42 17.93(0.05)	66 02 51.2(0.3)	13.8	80.6	203.2(19.)	<1.9	0.00	c
19034	15 42 18.43(0.06)	66 18 04.2(0.4)	7.2	51.0	68.8(10.)	<0.9	0.00	c
13012	15 42 21.89(0.07)	66 21 08.6(0.4)	9.2	46.5	73.3(11.)	<1.9	20.14	i
26014	15 42 21.68(0.04)	66 07 19.1(0.3)	10.3	277.4	589.3(41.)	12.0	25.55	i
13013	15 42 22.89(0.07)	66 22 24.2(0.4)	10.1	39.6	67.8(12.)	<1.9	0.00	b
26015	15 42 24.18(0.05)	66 10 05.5(0.3)	8.6	74.9	113.7(11.)	<1.2	0.00	i
26016	15 42 24.69(0.04)	66 10 12.3(0.2)	8.6	136.4	206.7(12.)	<0.9	19.68	i
26017	15 42 25.00(0.04)	66 09 17.3(0.2)	9.2	151.1	240.2(13.)	<0.9	21.32	i
19036	15 42 25.03(0.07)	66 13 06.3(0.4)	7.4	49.5	78.6(14.)	1.1x0p=38	0.00	c
19037	15 42 26.15(0.03)	66 15 39.1(0.2)	7.3	372.5	510.3(18.)	<0.4	0.00	i
13018	15 42 28.26(0.06)	66 22 02.8(0.3)	10.2	65.7	114.4(13.)	<1.0	0.00	b
26018	15 42 28.89(0.06)	66 02 56.4(0.4)	14.3	51.4	138.1(19.)	<2.1	25.43	i
19038	15 42 29.73(0.04)	66 14 27.3(0.2)	7.6	171.7	242.3(12.)	<0.5	21.45	i
19040	15 42 31.56(0.08)	66 14 26.8(0.5)	7.8	37.6	244.1(54.)	5.1x2.6p=156	18.57	i
19041	15 42 32.13(0.07)	66 16 19.6(0.4)	8.0	37.9	54.8(10.)	<1.7	22.18	i
19042	15 42 36.61(0.05)	66 11 04.7(0.3)	9.2	72.8	117.3(12.)	<1.1	0.00	c
26020	15 42 36.94(0.07)	66 05 13.3(0.4)	12.9	42.8	98.7(16.)	<1.3	0.00	b
26021	15 42 37.26(0.06)	66 02 44.8(0.4)	14.9	49.7	144.9(21.)	<1.3	21.26	i
19044	15 42 39.13(0.06)	66 13 26.2(0.4)	8.7	53.5	82.7(11.)	<1.1	19.51	i
19045	15 42 39.79(0.03)	66 18 35.9(0.2)	9.3	224.4	364.5(16.)	<0.7	0.00	b
26022	15 42 40.06(0.06)	66 07 03.1(0.4)	11.8	51.7	106.4(15.)	<1.6	0.00	c
13021	15 42 40.59(0.07)	66 26 40.0(0.4)	14.5	38.4	108.1(20.)	<1.4	24.72	i
13022	15 42 41.42(0.06)	66 24 33.7(0.4)	13.0	70.6	334.4(47.)	2.6x0.8p=111	19.51	i
13122	15 42 41.09(0.05)	66 24 36.7(0.3)	13.0	101.0	404.7(36.)	1.7x1.4p=127	18.75	i
13036	15 42 42.22(0.08)	66 20 36.7(0.5)	10.5	40.4	132.1(31.)	2.2x0.8p=162	20.20	i
19046	15 42 43.15(0.08)	66 15 05.8(0.5)	9.0	51.5	209.5(45.)	5.1x1.8p=6	22.90	i
26023	15 42 46.78(0.06)	66 08 41.4(0.3)	11.3	65.2	128.5(14.)	<1.2	24.64	i

Table 1—Continued

Name	RA(2000.0)	Dec(2000.0)	Dist Mpc	Peak μJy/b	Total μJy	Size arcsec	Rmag	ID
19049	15 42 47.61(0.03)	66 14 22.6(0.2)	9.4	417.3	690.8(24.)	<0.6	22.06	i
13024	15 42 49.46(0.07)	66 23 22.8(0.4)	12.7	41.8	94.8(16.)	<1.5	0.00	b
19050	15 42 51.21(0.07)	66 12 26.9(0.4)	10.1	44.1	77.9(13.)	<1.4	0.00	c
13026	15 42 51.61(0.04)	66 24 13.2(0.3)	13.4	114.4	281.2(19.)	<1.1	0.00	i
13027	15 42 51.79(0.08)	66 20 37.3(0.5)	11.3	42.5	146.2(33.)	2.2x1.2p=69	24.64	i
19051	15 42 52.50(0.07)	66 19 02.5(0.4)	10.7	43.1	77.6(13.)	<1.8	0.00	i
19052	15 42 53.18(0.06)	66 16 58.5(0.4)	10.2	56.0	99.0(13.)	<1.1	24.66	i
26025	15 42 54.38(0.04)	66 03 35.2(0.2)	15.3	226.5	801.1(39.)	1.1x0.5p=144	23.33	i
19053	15 42 54.38(0.06)	66 18 08.1(0.4)	10.6	54.4	99.8(13.)	<1.5	20.52	i
19054	15 42 54.64(0.07)	66 11 15.1(0.4)	10.8	38.1	69.4(13.)	<2.3	20.52	i
19055	15 42 55.98(0.07)	66 12 12.6(0.4)	10.7	62.2	148.3(22.)	1.5x0.5p=110	24.19	i
19056	15 42 58.49(0.08)	66 11 46.7(0.5)	11.0	37.8	103.9(26.)	1.8x0.8p=118	23.29	i
13028	15 42 59.97(0.03)	66 24 24.7(0.2)	14.2	277.6	795.2(33.)	0.8x0p=68	22.58	i
19058	15 43 01.07(0.03)	66 15 16.9(0.2)	10.8	386.0	729.3(26.)	<0.5	20.37	i
19060	15 43 05.79(0.07)	66 17 20.4(0.4)	11.5	42.7	83.1(14.)	<1.7	26.85	i
26026	15 43 08.89(0.03)	66 10 43.6(0.2)	12.4	382.0	852.2(30.)	<0.8	21.98	i
13031	15 43 09.31(0.06)	66 27 07.1(0.3)	16.7	65.3	245.0(27.)	<1.9	23.42	i
26027	15 43 09.43(0.08)	66 05 09.2(0.5)	15.3	34.8	108.8(22.)	<2.0	24.24	i
13032	15 43 09.84(0.02)	66 20 06.4(0.1)	12.7	1067.3	2458.7(76.)	<0.4	24.10	i
19063	15 43 10.49(0.04)	66 17 57.0(0.2)	12.1	141.3	305.4(18.)	<1.2	20.28	i
13033	15 43 11.44(0.04)	66 20 57.7(0.2)	13.2	187.2	509.3(31.)	1.5x0p=58	22.71	i
19064	15 43 12.16(0.07)	66 11 29.0(0.4)	12.4	42.4	95.5(16.)	<1.3	25.14	i
26028	15 43 12.75(0.05)	66 04 19.4(0.3)	16.1	74.1	257.6(26.)	<2.5	23.92	i
19065	15 43 13.41(0.05)	66 16 58.3(0.3)	12.2	103.7	227.0(17.)	<1.0	24.70	i
26029	15 43 13.71(0.06)	66 07 58.9(0.4)	14.0	67.5	229.0(31.)	1.4x0.7p=109	19.09	i
26030	15 43 14.01(0.05)	66 08 53.4(0.3)	13.6	82.7	211.7(19.)	<1.7	24.96	i
19067	15 43 14.63(0.07)	66 15 15.2(0.4)	12.1	35.1	76.9(16.)	<2.3	23.68	i